ARTICLE IN PRESS

Available online at www.sciencedirect.com
SCIENCE DIRECT®

Physics of the Earth and Planetary Interiors xxx (2004) xxx–xxx

PHYSICS OF THE EARTH AND PLANETARY INTERIORS

www.elsevier.com/locate/pepi

Thickness of the mantle transition zone beneath the South Pacific as inferred from analyses of ScS reverberated and Ps converted waves

D. Suetsugu [a,*], T. Saita [b], H. Takenaka [c], F. Niu [d]

[a] *Institute of Frontier Research on Earth Evolution, Japan Marine Science and Technology Center, 2-15 Natsushima-cho, Yokosuka, Kanagawa 237-0061, Japan*

[b] *Research Center for Seismology and Volcanology, Graduate School of Environmental Studies, Nagoya University, Furo-cho, Chigusa-ku, Nagoya City, Aichi Prefecture 464-8602, Japan*

[c] *Department of Earth and Planetary Sciences, Faculty of Sciences, Kyushu University, 6-10-1 Hakozaki, Higashi-ku, Fukuoka 812-8581, Japan*

[d] *Department of Earth Science, Rice University, 6100 Main Street, Houston, TX 77005, USA*

Received 2 September 2002; received in revised form 30 January 2003; accepted 18 June 2003

Abstract

We study the thickness of the mantle transition zone beneath the South Pacific in order to determine temperature anomalies associated with presumed hot plumes in the South Pacific Superswell. The ScS reverberation method is used to determine the average thickness between an event-station pair and the Velocity Spectrum Stacking (VSS) method is used to determine the thickness near each station. The thickness obtained by the ScS reverberation method shows that the average thickness beneath the Superswell is less than the globally averaged thickness by 6 km, while the average thickness beneath the Tonga–Fiji subduction is greater than the global average by 10 km. The VSS method shows nearly normal thickness beneath stations used in the Superswell region. We conclude that substantial thinning of the transition zone associated with presumed hot plumes occurs locally beneath the Society hot spot as revealed by our previous SS-precursor study, and is not widespread beneath the whole area of the Superswell.

Keywords: Superswell; Plumes; ScS-waves; Receiver function; Mantle; Transition zones

1. Introduction

The origin and nature of the hot spots in the South Pacific Superswell (McNutt and Fischer, 1987) are still controversial. The Superswell region has four hot spots (Marquesas, Pitcairn, Society, and Macdonald) with linear chains of volcanic islands and seamounts. Recent seismological studies have indicated a low-velocity (e.g., Resovsky and Ritzwoller, 1998; Ritsema and van Heijst, 2000; Masters et al., 2000; Zhao, 2001) and a low-Q (Romanowicz, 1995; Bhattacharyya et al., 1996; Suetsugu, 2001) in the mantle beneath the Superswell, suggesting the presence of high temperature and/or chemical anomalies associated with the uprising plumes at the hot spots. Global seismic tomography has the potential to constrain

* Corresponding author. Tel.: +81-468-67-9750; fax: +81-468-67-9745.
E-mail address: dai@jamstec.go.jp (D. Suetsugu).

0031-9201/$ – see front matter © 2004 Elsevier B.V. All rights reserved.
doi:10.1016/j.pepi.2003.06.008

thermal and chemical anomalies associated with the plumes, but cannot resolve the fine structure under the Superswell, because of the sparse distribution of earthquakes and seismic stations in the South Pacific.

The topography of the 410 and 660 km seismic discontinuities (called the "410" and the "660" hereafter) provides an alternative clue to understanding the thermal structure and the ascent process of hot plumes beneath the South Pacific, since the "410" and "660" are interpreted as the olivine-spinel and post-spinel phase changes, respectively. The "410" (and "660") are expected to be depressed (and elevated), in and near a hot plume since the olivine-spinel and the post-spinel phase changes have positive and negative Clapeyron slopes, respectively (Katsura and Ito, 1989; Ito and Takahashi, 1989). Recently, Niu et al. (2000, 2002) studied the topography of the "410" and "660" beneath the South Pacific to elucidate thermal anomalies associated with the presumed hot plumes. Niu et al. (2000) analyzed ScS reverberation from the "410" and "660" to determine the thickness of the mantle transition zone (called MTZ hereafter), which is defined as the depth interval between the "410" and "660." They showed that the average thickness of the mantle transition zone is less than the global average of 243 km (Gu et al., 1998) by 17 km beneath the South Pacific Superswell, although the ScS reverberations analyzed by Niu et al. (2000) did not sample the mantle transition zone densely under the Superswell because of the limited number (two) of earthquakes available at that time. Niu et al. (2002) analyzed SS-precursors reflected from the "410" and "660" to determine the topography of the "410 and "660." A striking result of Niu et al. (2002) is that the mantle transition is thinner by about 30 km than the global average locally beneath the Society hot spot but not very thin beneath the other three hot spots. We noticed that the SS data set used by Niu et al. (2002) has a low sampling density beneath the other three hot spots, however.

The purpose of the present study is to determine whether or not the low-velocity anomalies in the MTZ beneath the South Pacific Superswell is localized under the Society hot spot and whether or not the rest of the Superswell region has a nearly normal MTZ, using methods independent of those used by Niu et al. (2002). In the present paper, we employ the ScS reverberation method (Niu et al., 2000) and the Velocity Spectrum Stacking (VSS) method (Gurrola et al., 1994; Saita et al., 2002; called VSS hereafter) to constrain the thickness of the MTZ beneath the South Pacific Superswell. In the ScS reverberation method, we augment four more earthquakes to the data set used by Niu et al. (2000) to improve the spatial coverage of the points sampled by the ScS reverberation waves.

2. Data and method

The two methods used in the present study are complementary. The ScS reverberation method is useful to obtain the average thickness of the MTZ at the reflection points of the ScS reverberated waves along the great circle between an event and a station (e.g., Revenaugh and Jordan, 1987; Ohtaki et al., 2002). The VSS, on the other hand, is used to estimate the MTZ thickness within a radius of 100–300 km from a station. We analyzed waveform data recorded at broadband stations of SPANET (South Pacific Broadband Seismic Network) (Ishida et al., 1999), IRIS (Incorporated Research Institutions for Seismology), and LDG/CEA (Laboratoire de Geophysique, the French Commissariat l'Energie Atomique) in the South Pacific (Fig. 1). For the ScS reverberation method, we analyzed a total of six Fiji–Tonga–Kermadec events from 1996 to 2001 with depths greater than 500 km (Fig. 1 and Table 1) which produced multiple ScS-waves efficiently. For the VSS method, we selected events with a body wave magnitude mb $>$ 6 which took place between 1995 and 2001 which had epicentral distance ranging 40–95° from the stations. We visually inspected 100–150 seismograms for each station, and then discarded data with low *S*/*N* ratios. Only six stations (PPT, RKT, TBI, LBSA, NIUE, and NRFK; see Fig. 1) were left for further analysis. The number of

Table 1
Events analyzed by the ScS reverberation method (after PDE)

Origin time	Latitude	Longitude	Focal depth (km)	M_w
August 5, 1996	20.69°S	178.31°W	550	7.4
September 4, 1997	26.57°S	178.34°E	624	6.8
March 29, 1998	17.55°S	179.09°W	537	7.2
April 14, 1998	23.82°S	179.87°W	550	6.1
May 16, 1998	22.23°S	179.52°W	586	6.9
December 18, 2000	21.18°S	179.12°W	628	6.7

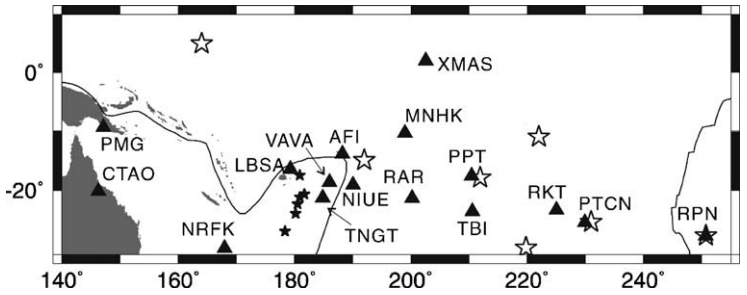

Fig. 1. A map showing earthquakes (solid star), broadband seismic stations (solid triangle) used in the present study. Hot spots in the studied area are denoted by open star.

records used is 52, 32, 61, 21, 13, and 22 for PPT, RKT, TBI, LBSA, NIUE, and NRFK, respectively. Most of the selected events were located from the Fiji–Tonga region to Indonesian regions, and the Izu–Japan–Kuril region, and some from the central and South America, resulting in Ps conversion points at the transition zone discontinuities located to the west and northwest mostly and to the east for a few events, within 300 km from each station.

2.1. The ScS reverberation method

The ScS reverberations are ScS-waves reflected at either the upper-side (arriving from above) or the under-side (arriving from below) of a discontinuity (e.g., Revenaugh and Jordan, 1987), which are useful for the determination of the depth of discontinuities in the mantle. On a single seismogram, ScS*n* phases of different reflection number n have similar propagation paths near their endpoints, so that analyzing ScS*n* phases can reduce the effects of instrument response and of heterogeneities near the source and receivers. Fig. 2 illustrates the two series of ScS reverberated waves for the case of $n = 3$. As shown in this figure, there are two series of ScS reverberated waves, the upper-side reflection ScS*n*_*d*+ and the under-side reflection ScS*n*_*d*−, for a mantle discontinuity (where '*d*' is the depth of the discontinuity; '+' and '−' represent the upper-side and under-side reflection, respectively). The ScS*n*_*d*− phases arrive before their parent phase ScS*n*, while the ScS*n*_*d*+ phases arrive after their parent phase sScS*n*.

Fig. 3 shows the flow of the ScS reverberation method. We select ScS*n* and sScS*n* phases which are well separated from other phases such as SSS and which have a high *S*/*N* ratio. In the present study we use $n = 1$–3 for sScS*n* and $n = 2$–4 for ScS*n*. The horizontal components are rotated to a tangential-component seismogram and bandpass-filtered at frequencies between 0.01 and 0.05 Hz, which are used in the further analysis. We divide the seismogram into time series

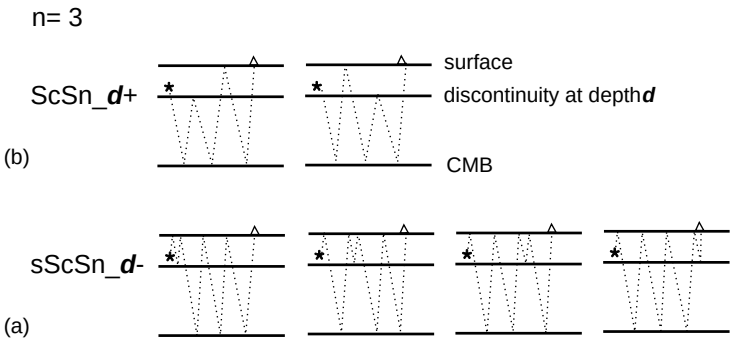

Fig. 2. Schematic illustration of the ray path of (a) ScS3_*d*−, and (b) sScS3_*d*+, where '*d*' is the depth of the discontinuity. '+' and '−' represent the upperside and under-side reflections, respectively. Star and triangle represent the event and station, respectively.

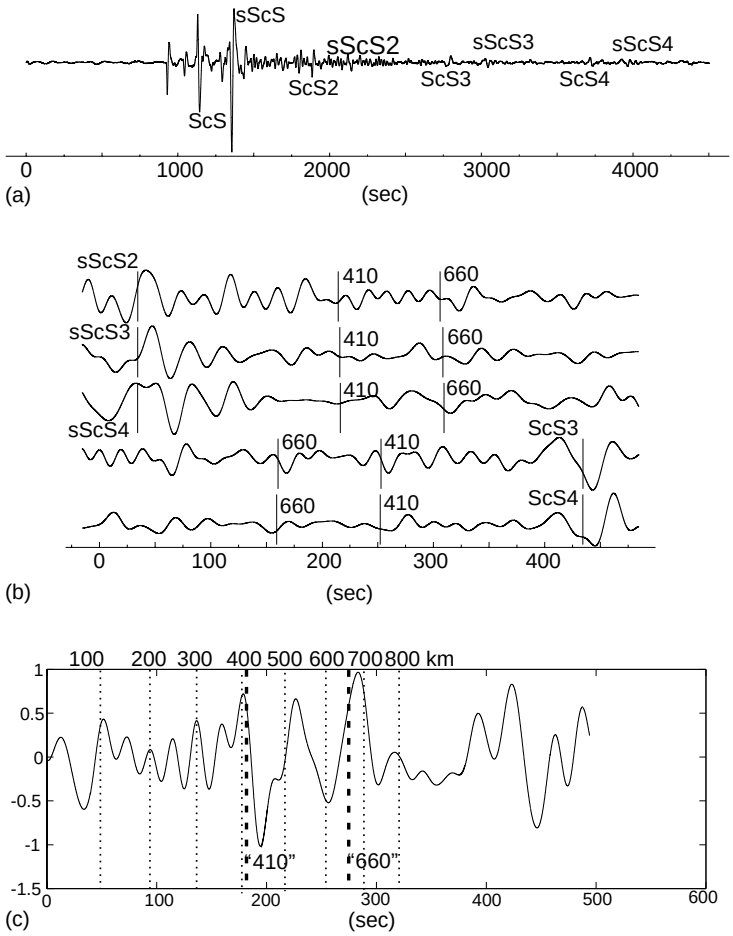

Fig. 3. An example of the ScS reverberation method. (a) Transverse-component seismogram filtered from 0.01 to 0.05 Hz. (b) Windowed seismograms for sScS*n* ($n = 2$–4) and ScS*n* ($n = 3$, 4). Each window includes reflected waves at the "410 and "660" as later phases for sScS*n* waves and precursors for ScS*n* waves. (c) Stacked seismogram to enhance the reflected waves. The lower horizontal axis is the time and the vertical dotted lines are the P to S conversion depths with the 100 km interval, which is computed using the Iasp91 model. The thick dashed lines denote depths of 410 and 660 km.

containing the reverberations and their parent phase. Because ScS*n*_*d*− waves arrive before ScS*n*, and sScS*n*_*d*+ waves come after sScS*n*, we reverse the ScS*n* series in time. We deconvolve the time series with the parent phase, and stack them for each station after the necessary moveout corrections calculated by 1D ray tracing for ScS*n*_*d*− and ScS*n*_*d*+ using the Iasp91 model (Kennett and Engdahl, 1991). Because ScS*n*_*d*− has polarity opposite to ScS*n*_*d*+, we reverse the polarity of the sScS*n* seismograms. Fig. 3c shows the stacked seismograms, from which we pick the arrival times of the peaks nearest to those expected for reflectors at depths of 410 and 660 km to calculate the depths of the discontinuities and the thickness of the MTZ using the Iasp91 model. The discontinuity depth thus determined represents the average depth at the reflection points for an event-station pair.

2.2. The VSS method

Teleseismic P-wave energy is partially converted to S-waves at velocity discontinuities beneath stations. Differences in arrival times between the direct

P-wave and the Ps converted wave are a function of the discontinuity depth and the P and S velocities above the discontinuity. Following Gurrola et al. (1994) and Saita et al. (2002) we obtained the "410" and "660" near stations in the studied area by the VSS method. First we compute a receiver function by deconvolving the vertical-component record from the radial-component record for each event at each station to equalize the source effect (e.g., Owens and Crosson, 1988). We used a Gaussian filter of $G(f) = \exp[-(ft_p)^2]$ with t_p of 8 s in the deconvolution in order to reduce the oceanic noise from 1 to 10 s. We further applied attenuation filters of Q_p and Q_s in the upper mantle to the radial and vertical component records, respectively, before the deconvolution in order to reduce the effect of differential attenuation of P and Ps waves on the receiver function (Saita et al., 2002). The Q values are taken from PREM (Dziewonski and Anderson, 1981). The amplitudes of the Ps converted waves in individual receiver functions are often comparable to or below the noise level. We, therefore, stacked the receiver functions with a moveout correction to enhance the Ps waves. The moveout correction is computed for discontinuity depths from 0 to 800 km with grid interval of 1 km and for S-wave velocities perturbed from −2.5 to +2.5% with respect to the Iasp91 model with grid interval of 0.1%. In the moveout correction we assumed $\mathrm{d}\ln V_s/\mathrm{d}\ln V_p = 1.5$ (Zhou and Clayton, 1990).

The presence of Ps converted waves is indicated by large stacked amplitudes at appropriate depths and velocities on the plot of the stacked amplitude versus S-velocity perturbation and conversion depth (the VSS plot). Fig. 4 is the VSS plot for the station TBI (Tubuai) in the Macdonald hot spot chain. If the conversion depth and S-velocity perturbation is well resolved, we would observe a peak of the stacked amplitude at an appropriate depth and a velocity perturbation. Fig. 4 shows, however, high amplitude ridges rather than peaks, suggesting that the depths and the velocity perturbation have a strong trade-off and thus cannot be determined independently (Gurrola and Minster, 1998). We, therefore, rely on the existing global three-dimensional S-velocity model obtained by Su et al. (1994) to account for S-velocity

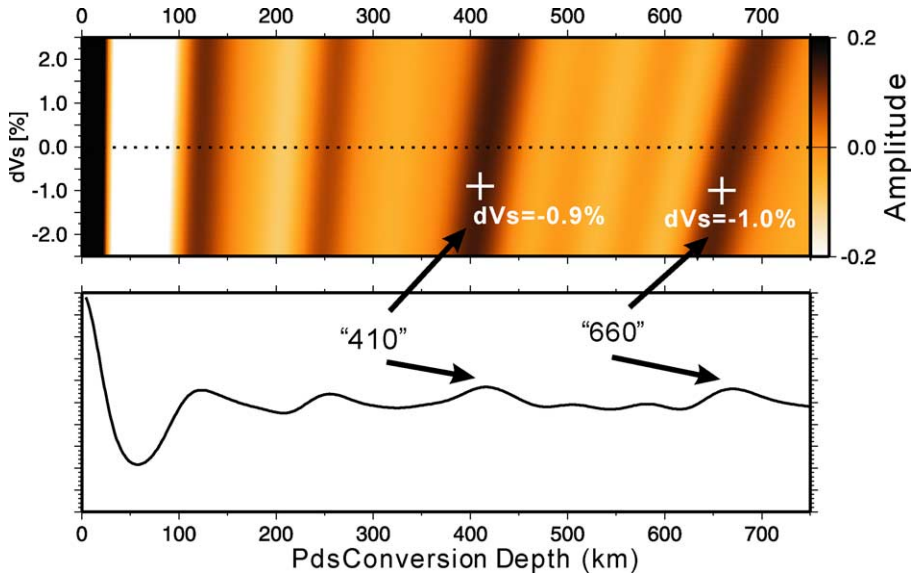

Fig. 4. A Velocity Spectrum Stacking plot for the station TBI on Tubuai Island in French Polynesia (top). Amplitudes of stacked receiver functions are normalized to 20% of the direct P-wave amplitudes and shown with respect to the Ps conversion depths and the average S-wave velocity perturbations above the conversion depths. The "410" and "660" depths of 410 and 659 km, shown as plus, are determined using the average velocity perturbations of a tomographic model by Su et al. (1994). The stacked seismogram using the Iasp91 model is also shown (bottom).

perturbations above the conversion depths below the stations. The MTZ thickness is obtained by subtracting the "410" depth from the "660" depth at each station. The estimation errors are computed independently for the "410" and the "660," and the MTZ thickness using the bootstrap method (e.g., Efron and Tibshirani, 1986) which randomly re-samples (4000-times) the receiver functions for each station prior to the stacking. In the present paper we will show the MTZ thickness, rather than the "410" and "660" depths, because the thickness is little affected by strongly heterogeneous upper mantle (above the "410") velocity structure.

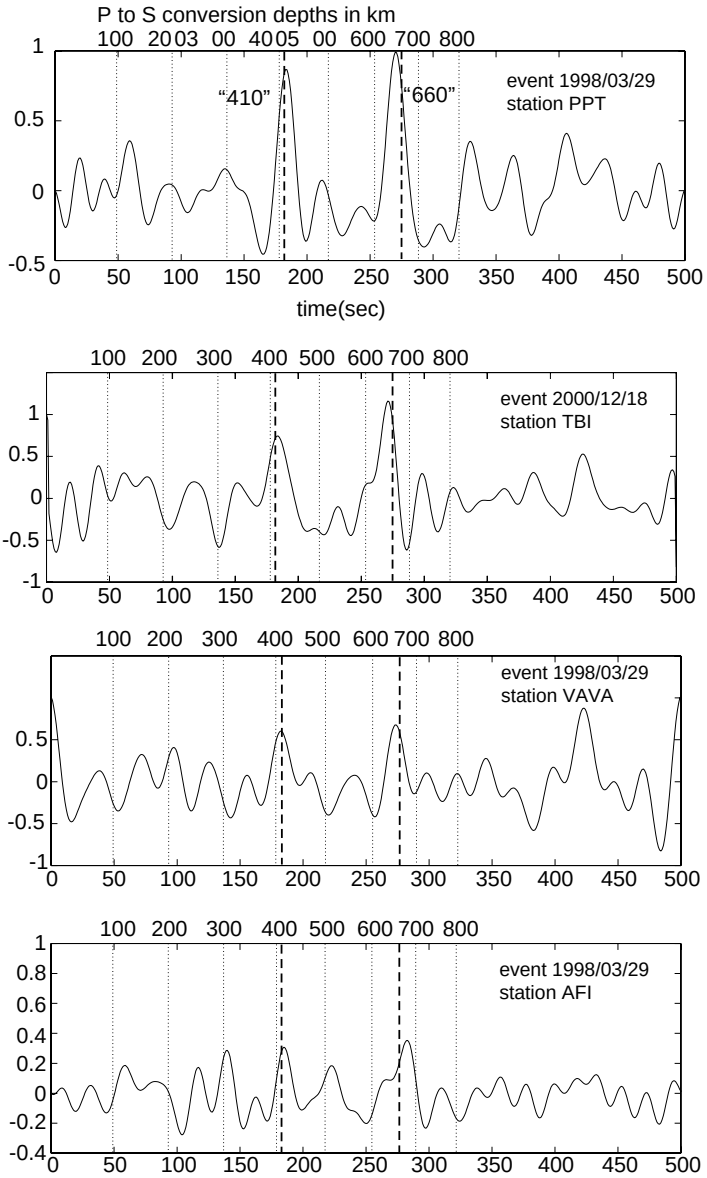

Fig. 5. Examples of the stacked seismograms of the ScS reverberated waves. The top two traces are obtained from event-station pairs of which ScS-reverberated waves sample the MTZ under the South Pacific Superswell and the bottom two are those sampling the Tonga–Fiji subduction zone. The convention of the diagram is the same as that in Fig. 3c.

3. Results

3.1. MTZ thickness from the ScS reverberations

Examples of the stacked traces obtained by the ScS reverberation method are shown in Fig. 5, whose top two traces have the reflection points at the ‘’410” and “660” in the Superswell (PPT and TBI) and the bottom two in the Tonga–Fiji subduction zone (VAVA and AFI). The interval of peaks for the “410” and “660” is shorter for the stacked traces for the stations in the Superswell than those for the stations in the Tonga–Fiji subduction zone, suggesting a thinner MTZ beneath the Superswell than beneath the subduction zone. Fig. 6 shows the geographical distribution of the MTZ thickness perturbation from the global average of 243 km which was determined by Gu et al. (1998). The MTZ beneath the Tonga–Fiji subduction zone is 253 ± 9 km, which is estimated from the stations in the subduction zone (TNGT, VAVA, NIUE, and AFI) and is thicker than the average by 10 km. In contrast, the average MTZ thicknesses beneath the Superswell is 237 ± 4 km, which is obtained from stations in the Superswell region (PPT, RAR, MNHK, RPN, PTCN, RKT, and TBI). The MTZ is slightly but consistently thinner than the global average by about 6 km, suggesting that the MTZ is warmer than the global average under the Superswell.

3.2. MTZ thickness from the VSS method

Fig. 7 shows the VSS plots obtained by the present study, in which there are ridges in the P to S conversion energy at the “410” and “660.” Beside the amplitude ridges corresponding to the “410” and “660,” there are several ridges shallower than 400 km, most of which can be attributed to crustal reverberations. The subduction zone stations (LBSA, NIUE, NRFK) give two or three ridges between the “410” and “660,” while the VSS from the Superswell stations does not have significant energy between the two discontinuities. In particular, all the subduction zone stations indicate a ridge at depths from 500 to 550 km, which may be the conversion energy from the 520-km discontinuity (e.g., Flanagan and Shearer, 1998), while the PTCN station located away from subduction zones also shows the converted signal at around 520 km. We need more data for the subduction zone to make sure that these ridges are real, because the number of stacked traces for the subduction zone is less than that for the Superswell stations. The geographical distribution of the MTZ thickness obtained by the VSS method is shown in Fig. 8. The MTZ near the Tonga–Fiji subduction zone is estimated at the LBSA station in Fiji to be thicker than the average by 13 km, which is consistent with the results obtained by the ScS reverberation method described above. The NIUE station, which is located immediately east of the Tonga–Fiji subduction

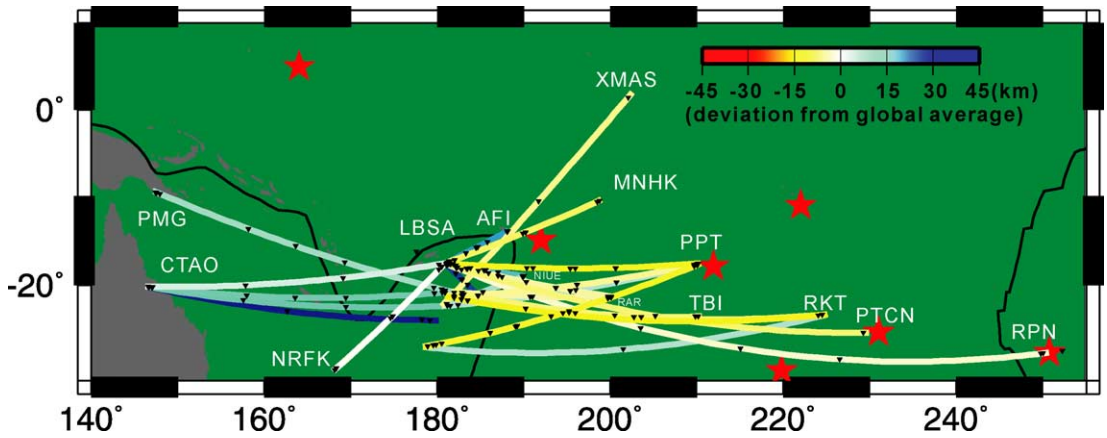

Fig. 6. The thickness of the transition zone calculated from the depths of the 410 and 660 km discontinuities. The deviation from the global average obtained by Gu et al. (1998) is shown. Stars and triangles represent the hot spots and the reflection points of the ScS reverberated waves, respectively.

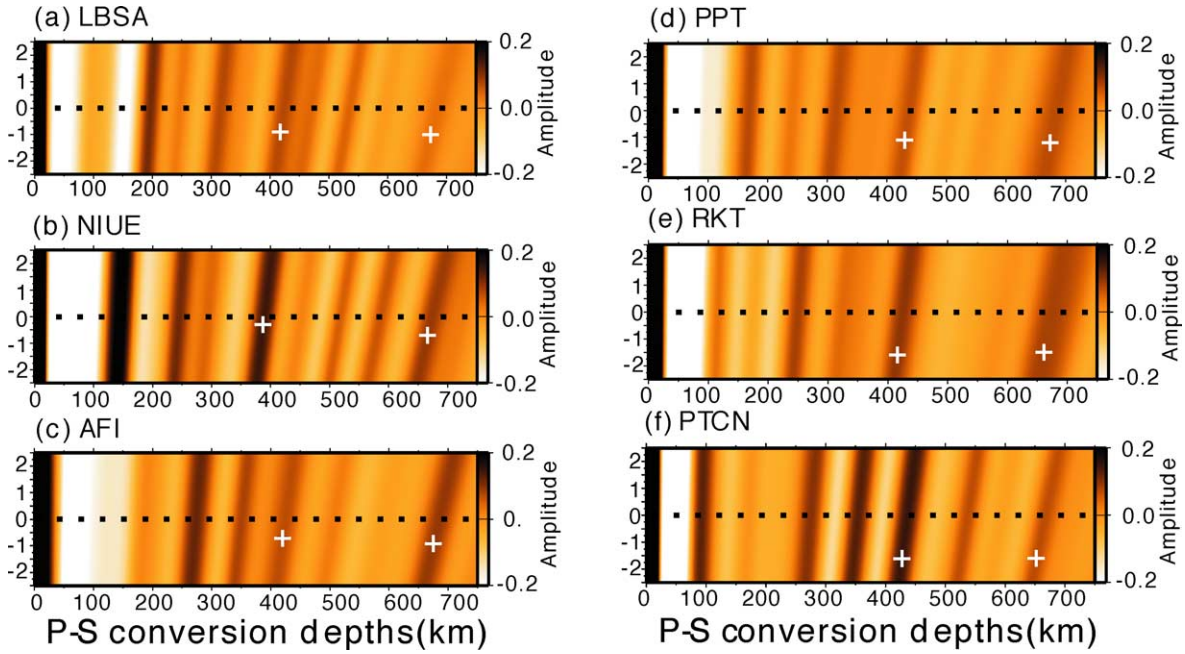

Fig. 7. The VSS plots obtained by the present study. The convention of the diagram is the same as in Fig. 4.

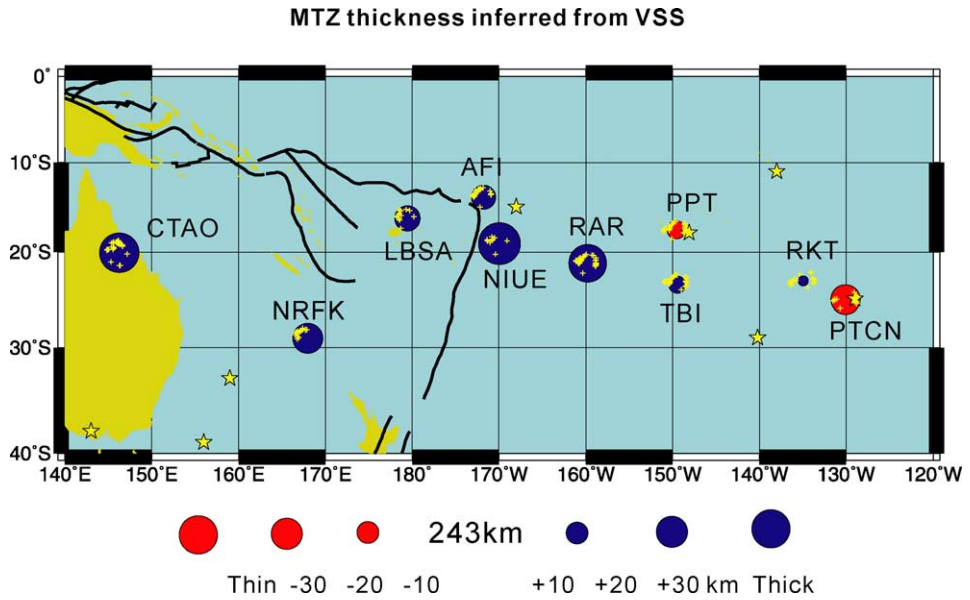

Fig. 8. A map showing the MTZ thickness obtained by the VSS method. The deviation from the global average obtained by Gu et al. (1998) is shown. The yellow plus represents the P to S conversion points.

Table 2
Thickness of the mantle transition zone obtained by the VSS method

Station	Thickness (km)	Standard error (km)	Number of events
CTAO	275	3	69
AFI	255	29	34
LBSA	256	19	21
NIUE	279	11	13
NRFK	262	9	22
RAR	272	12	54
TBI	249	4	61
PPT	236	9	59
RKT	245	13	32
PTCN	225	9	18

zone, gives an estimate of the MTZ thicker than the average by 36 km, while it is relatively less reliable because of the small number of available data at NIUE. The MTZ beneath the stations in the Superswell is thinner than Tonga–Fiji subduction zone and near the global average except for PTCN on Pitcairn Island (225 ± 9 km). It is 236 ± 9 km at PPT near the Society hot spot, 245 ± 12 km at RKT on Gambier Island in the Pitcairn hot spot chain, and 249 ± 16 km at TBI on Tubuai Island in the Macdonald hot spot chain (Table 2).

4. Discussion and conclusions

Potential sources of uncertainty in the "410" and "660" depths include errors in the upper mantle velocity model, crustal model, and attenuation structure. All of these could introduce baseline offsets in both of the depth estimates. The MTZ thickness, which is computed from the two depth estimates, is much less affected by such errors. However, if the MTZ has substantially low-velocity anomalies and strong attenuation, which may be associated with upwelling plumes beneath the Superswell, they could affect the results of the present study. We estimated a systematic error caused by low velocities and low Q_s using synthetic seismograms with Direct Solution Method (Cummins et al., 1994). Recent shear velocity models consistently show slow velocities in the MTZ beneath the Superswell, while the degree of the low velocities ranges from -0.2 to -1.8% (e.g., Su et al., 1994; Masters et al., 2000; Mégnin and Romanowicz, 2000; Ritsema and van Heijst, 2000). Recent attenuation studies indicate that the shear Q is from 80 to 100 in the upper mantle beneath the Superswell (e.g., Romanowicz, 1995; Bhattacharyya et al., 1996; Suetsugu, 2001). First we assessed the possible error in the MTZ thickness obtained by the ScS reverberation method. We computed tangential-component seismograms by assuming the Iasp91 model and Q_s of 80 throughout the upper mantle, then applied the ScS reverberation method to the synthetics. The MTZ thickness thus obtained is greater than that of the Iasp91 model (250 km) by 4 km. To estimate a systematic error caused by low-velocity anomalies, we calculated the synthetic seismograms assuming the Iasp91 model with the upper mantle S-velocities reduced by 1%. The MTZ thickness obtained from the synthetics is greater than that of the Iasp91 model by 5 km. Combining the errors caused by the low-velocity and low Q_s, the MTZ thickness obtained by the ScS reverberation method could be overestimated by 9 km in maximum. Regarding with the VSS method, we have already taken the low-velocity anomalies of 1–1.5% into account using the shear velocity model by Su et al. (1994). From Fig. 7, we can estimate the effect of the velocity correction by 1% on the MTZ thickness is 3 km. We examined the effect of low Q_s of 80 on the MTZ thickness estimated by the VSS method. The synthetic seismograms are computed by assuming the low Q_s in the upper mantle and analyzed with the VSS method by correcting for the attenuation effect with the PREM Q_s model. The MTZ thickness thus obtained is 6 km greater than that of the Iasp91 model. In summary, assuming the low V_s and low Q_s, we could obtain the MTZ thinner than the results shown in the previous section, but the systematic error is less than 10 km, which does not significantly affect our conclusions.

The structure of the MTZ has not been well documented beneath the South Pacific, particularly in the Superswell region. Roth and Wiens (1999) studied the MTZ underneath the Tonga–Fiji subduction zone using the ScS reverberation method. They showed that the thickness of the MTZ beneath the Tonga–Fiji subduction zone varies laterally and that it is as thick as 265 km directly beneath and to the west of the subduction zone, which is thicker than the global average by 22 km. The present study shows thicker than average MTZ at all studied locations beneath the Tonga–Fiji subduction zone as shown by both the ScS

reverberation and VSS method. Vinnik et al. (1997) employed a receiver function method to estimate the time interval between P660s and P410s at broadband stations in the South Pacific. Among the stations used in their study, the time interval at PPT is 26.7 ± 1.4 s for a reference ray parameter of 6.4 s per degree, which can be translated to about 270 ± 15 km, much thicker than the thickness of 236 ± 9 km obtained by the present study. Differences in the methodologies of the two studies (the velocity correction, the attenuation correction, and so forth) cannot account for the large difference in the obtained MTZ thickness and the reason of the discrepancy remains unclear. The moderately thin MTZ beneath PPT obtained by the present study is in good agreement with the results by the previous global MTZ studies using the SS-recursors (Flanagan and Shearer, 1998; Gu et al., 1998) in which the average thickness of the MTZ beneath the Superswell region is thinner than the global average by 5–10 km and to the west of the trench (the Tonga–Fiji subduction zone and the Coral Sea) the MTZ is thicker than the average by 10–20 km.

Recently, Niu et al. (2002) analyzed differential travel times between SS and its under-side reflections from the "410" and "660" beneath the South Pacific Superswell. They found that the MTZ is about 30 km thinner than the global average over an area 500 km or less in diameter beneath the Society hot spot near PPT (Fig. 9). The MTZ is not thinned beneath the other hot spots in the Superswell area, while the coverage of the SS-precursors is worse around the other hot spots than around the Society hot spot. The thinning of the MTZ beneath the Superswell estimated by the present study is about 6 km, which is much less than that beneath the Society hot spot obtained by Niu et al. (2002). The ScS reverberation analysis of the present study provides the MTZ thicknesses which are averaged over the reflection points of the ScS reverberated waves for each event-station pair. The ScS reverberated waves could miss the localized thin MTZ zone beneath the Society hot spot found by Niu et al. (2002), since the reflection points are not located in or near the very thin MTZ, as shown in Fig. 9. The MTZ thickness obtained by the present ScS reverberation method is thus regarded as the average thickness of the MTZ outside the localized thin MTZ. Niu et al. (2002) indicated that the average thickness of the MTZ beneath the entire Superswell region is 237 ± 5 km, which is same

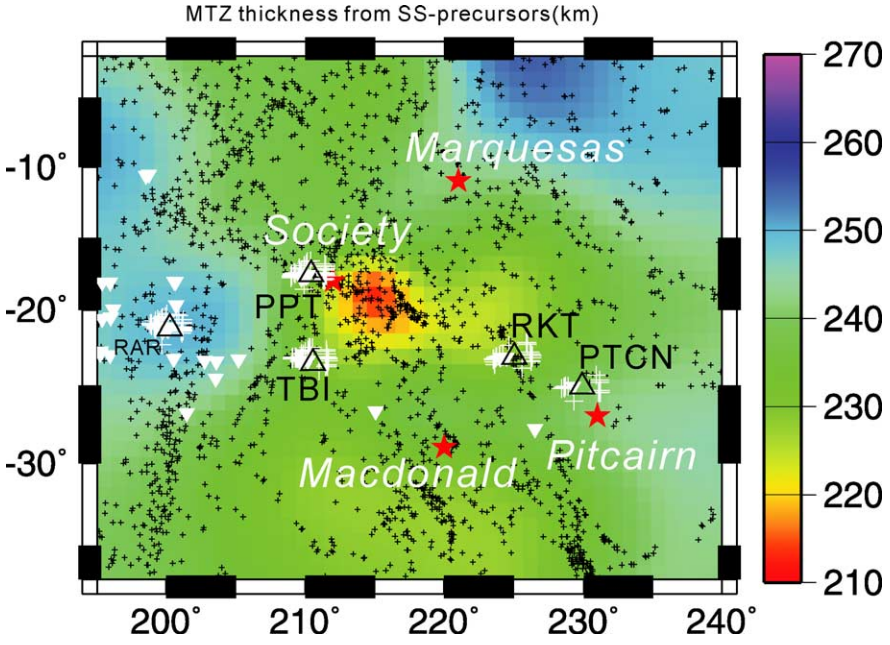

Fig. 9. A map of the South Pacific Superswell showing the MTZ thickness obtained by SS-precursor analysis (Niu et al., 2002). Black plus, white plus, and white triangle represent the bounce points of SS waves, the P to S conversion points at the "410," and the reflection points of the ScS reverberated wave at the "410," respectively. Hot spots are denoted by red stars.

as our estimate in the same region (237 ± 4 km). The VSS approach in the present study does not show substantially thinned MTZ either beneath the Superswell except for PTCN. It is also because the Ps converted waves analyzed in the VSS method miss the localized thin MTZ zone. The conversion points of P410s waves observed at PPT are located near the localized thin MTZ but not in it (Fig. 9), which gives us only moderately thin MTZ thickness (236 km). The conversion points for the other two stations (TBI and RKT) are located far outside the localized thin MTZ. We need more data to conclude that the substantially thinned MTZ beneath PTCN (225 km) is real, since the data coverage of the SS-precursors and the number of data for the VSS method are worst among the stations in the Superswell (Table 2 and Fig. 9). The thickness of the MTZ near the conversion points are 240–250 km, which are close to the thickness computed by the VSS method.

If we suppose that the temperature anomaly at the "410" is the same as that at the "660," we can then compute the temperature anomalies of the transition zone beneath the South Pacific using published values of the Clapeyron slopes. To translate the MTZ thickness deviation to the temperature anomaly, we use the Clapeyron slopes of 2.5–2.9 MPa/K and −3.0 to −2.0 MPa/K for the olivine-β-spinel and the post spinel phase changes, respectively (Bina and Helffrich, 1994). We estimate that the average temperature anomaly in the MTZ over Superswell is +50 K at maximum from the ScS reverberation results and the local temperature deviation from the global average determined from the VSS method are within 50 K. The average temperature anomaly beneath the Tonga–Fiji subduction zone is −100 to −70 K from the ScS reverberation results.As a conclusion, beneath the South Pacific Superswell, both the average thickness of the MTZ determined from the ScS reverberation method and the thickness near the stations in the Superswell region obtained by the VSS method are not substantially less than the global average: The MTZ is only moderately thinner than the global average. Combining the results of the present study with the substantial thinning beneath the Society hot spot found by Niu et al. (2002), we conclude that high temperature anomalies associated with presumed hot plumes are localized rather than of a large lateral dimension. Seismic tomographic studies commonly indicate an extensive low-velocity anomaly of several thousand kilometers in horizontal dimension at the lowermost mantle (e.g., Ritsema and van Heijst (2000); Masters et al., 2000) and some studies show a low-velocity zone of 1000–1500 km in diameter throughout the lower mantle (e.g., Resovsky and Ritzwoller, 1998; Zhao, 2001) beneath the South Pacific Superswell. It is still unresolved how the extensive low-velocity zone in the lower mantle is related to the high-temperature signature in the MTZ (Niu et al., 2002) and hot spots in the Superswell region. Deployment of dense seismic arrays on oceanic islands (Ishida et al., 1999; Barruol et al., 2002) and on ocean bottom in the Superswell region is required to improve the spatial resolution of the tomographic image of the mantle and topography of the mantle discontinuities in the South Pacific Superswell.

Acknowledgements

We thank S. Sekiguchi and T. Negishi for operating the data center and making the SPANET data easily available to us and the IRIS DMC for providing the IRIS data in a user friendly manner. I would like to thank the Laboratoire de Geophysique for allowing me to analyze their valuable data and D. Reymond for helping me to collect the data. I thank Robert Geller, G. Helffrich, and G. Barruol for critically reading the manuscript and providing valuable comments. We used the GMT mapping tool (Wessel and Smith, 1998) to make figures. The VSS work is a part of T. Saita's Ph.D. thesis at Kyushu University. This work was done under the Superplume Project, which was funded by the Science and Technology Agency (now the Ministry of Education, Culture, Sports, Science and Technology) of the Government of Japan.

References

Barruol, G., Bosch, D., Clouard, V., Debayle, E., Doin, M.-P., Fontaine, F., Godard, M., Masson, F., Reymond, D., Tommasi, A., Thoraval, C., 2002. PLUME investigates the South Pacific Superswell. EOS 83, 511–514.

Bina, C., Helffrich, G., 1994. Phase transition Clapeyron slopes and transition zone seismic discontinuity topography. J. Geophys. Res. 99, 15853–15860.

Bhattacharyya, J., Masters, G., Shearer, P., 1996. Global lateral variations of shear wave attenuation in the upper mantle. J. Geophys. Res. 101, 22273–22289.

Cummins, P.R., Geller, R.J., Takeuchi, N., 1994. DSM complete synthetic seismograms: P-SV, spherically symmetric, case. Geophys. Res. Lett. 21, 1663–1666.

Dziewonski, A., Anderson, D.L., 1981. Preliminary reference Earth model. Phys. Earth Planet. Int. 25, 297–356.

Efron, B., Tibshirani, R., 1986. Bootstrap methods for standard errors, confidence intervals, and other measures of statistical accuracy. Stat. Sci. 1, 54–77.

Flanagan, M., Shearer, P., 1998. Global mapping of topography on transition zone velocity discontinuities by stacking SS precursors. J. Geophys. Res. 103, 2673–2692.

Gu, Y., Dziewonski, A.M., Agee, C.B., 1998. Global de-correlation of the topography of transition zone discontinuities. Earth Planet. Sci. Lett. 157, 57–67.

Gurrola, H., Minster, J.B., Owens, T., 1994. The use of velocity spectrum for stacking receiver functions and imaging upper mantle discontinuities. Geophys. J. Int. 117, 427–440.

Gurrola, H., Minster, J.B., 1998. Thickness estimates of the upper mantle transition zone from bootstrapped velocity spectrum stacks of receiver functions. Geophys. J. Int. 133, 31–43.

Ishida, M., Maruyama, S., Suetsugu, D., Matsuzaka, S., Eguchi, T., 1999. Superplume Project: towards a new view of whole earth dynamics. Earth Planet. Space 51, 1–5.

Ito, E., Takahashi, E., 1989. Postspinel transformations in the system Mg_2SiO_4–Fe_2SiO_4 and some geophysical implications. J. Geophys. Res. 94, 10637–10646.

Katsura, T., Ito, E., 1989. The system Mg_2SiO_4–Fe_2SiO_4 at high pressures and temperatures: precise determination of stabilities of olivine, modified spinel, and spinel. J. Geophys. Res. 94, 15663–15670.

Kennett, B.L.N., Engdahl, E.R., 1991. Traveltimes for global earthquake location and phase identification. Geophys. J. Int. 105, 429–465.

Masters G., Laske, G., Bolton, H., Dziewonski, A., 2000. The relative behavior of shear velocity, bulk sound speed, and compressional velocity in the mantle: implications for chemical and thermal structure. In: Karato, S., Forte, A.M., Liebermann, R.C., Masters G., Stixrude, L. (Eds.), Earth's Deep Interior: AGU Monograph 117. AGU, Washington DC.

McNutt, M.K., Fischer, K.M., 1987. The South Pacific Superswell. In: Keating, B.H., Fryer, P., Batiza, R., Boehlert, G.W. (Eds.), Seamounts, Islands, and Atolls, Geophysical Monograph Series, 43. American Geophysical Union, Washington, DC, pp. 25–43.

Mégnin, C., Romanowicz, B., 2000. The three-dimensional shear velocity structure of the mantle from the inversion of body, surface and higher-mode waveforms. Geophys. J. Int. 143, 709–728.

Niu, F., Inoue, H., Suetsugu, D., Kanjo, K., 2000. Seismic evidence for a thinner mantle transition zone beneath the South Pacific Superswell. Geophy. Res. Lett. 27, 1981–1984.

Niu, F., Solomon, S.C., Silver, P.G., Suetsugu, D., Inoue, H., 2002. Mantle transition-zone structure beneath the South Pacific Superswell and evidence for a mantle plume underlying the Society hot spot. Earth Planet. Sci. Lett. 198, 371–380.

Ohtaki, T., Suetsugu, D., Kanjo, K., Purwana, I., 2002. Evidence for a thick mantle transition zone beneath the Philippine Sea from multiple-ScS waves recorded by JISNET. Geophys. Res. Lett. 29, doi: 10.1029/2002GL014764.

Owens, T.J., Crosson, R.S., 1988. Shallow structure effects on broadband teleseismic P waveforms. Bull. Seismol. Soc. Am. 78, 96–108.

Resovsky, J.S., Ritzwoller, M.H., 1998. A degree 8 mantle shear velocity model from normal mode observations below 3 MHz. J. Geophys. Res. 104, 993–1014.

Revenaugh, J., Jordan, T.H., 1987. Observations of first-order mantle reverberations. Bull. Seismol. Soc. Am. 77 (5), 1704–1717.

Ritsema, J., van Heijst, H.J., 2000. Seismic imaging of structural heterogeneity in Earth's mantle: Evidence for large-scale mantle flow. Sci. Prog. 83, 243–259.

Romanowicz, B., 1995. A global tomographic model of shear attenuation in the upper mantle. J. Geophys. Res. 100, 12375–12394.

Roth, E.G., Wiens, D.A., 1999. Depression of the 660 km discontinuity beneath the Tonga slab determined from near-vertical ScS reverberations. Geophys. Res. Lett. 26, 1223–1226.

Saita, T., Suetsugu, D., Ohtaki, T., Takenaka, H., Kanjo, K., Purwana, I., 2002. Transition zone thickness beneath Indonesia as inferred using the receiver function method for data from the JISNETS regional broadband seismic network. Geophys. Res. Lett. 29, doi: 10.1029/2001GL013629.

Su, W.J., Woodward, R.L., Dziewonski, A.M., 1994. Degree 12 model of shear velocity heterogeneity in the mantle. J. Gephys. Res. 99, 6945–6980.

Suetsugu, D., 2001. A low Q_{ScS} anomaly near the South Pacific Superswell. Geophys. Res. Lett. 28, 391–394.

Vinnik, L., Chevrot, S., Montagner, J.-P., 1997. Evidence for a stagnant plume in the transition zone? Geophys. Res. Lett. 24, 1007–1010.

Wessel, P., Smith, W.H.F., 1998. New, improved version of the Generic Mapping Tools released. EOS Trans. AGU 79, 579.

Zhao, D., 2001. Seismic structure and origin of hot spots and mantle plumes. Earth Planet. Sci. Lett. 192, 251–265.

Zhou, H., Clayton, R.W., 1990. P and S wave travel time inversions for subducting slab under the island arcs of the northwest Pacific. J. Geophys. Res. 95, 6829–6851.